Cancer Nanotechnology

RESEARCH Open Access

Collagen-induced assembly of adenosine monophosphate-modified gold nanoparticles for photothermal cancer therapy

Xinyu Qu[1†], Yixing Chen[1†], Zhuyun Cai[2†], Xinyu Zhao[1*], Hua Zeng[1], Xiaohao Liu[1], Shuo Tan[1], Bingqiang Lu[1], Rui Gao[2*] and Feng Chen[1,3*]

†Xinyu Qu, Yixing Chen and Zhuyun Cai have equally contributed to this work

*Correspondence: xyzhao@tongji.edu.cn; gaoruidr@hotmail.com; fchen@tongji.edu.cn

[1] Center for Orthopaedic Science and Translational Medicine, Department of Orthopaedics, Shanghai Tenth People's Hospital, School of Medicine, Tongji University, 301 Yanchang Road, Shanghai 200072, People's Republic of China
[2] Department of Orthopedics, Second Affiliated Hospital of Naval Medical University, 415 Fengyang Road, Shanghai 200003, People's Republic of China
[3] National Engineering Research Center for Nanotechnology, Shanghai 200241, People's Republic of China

Abstract

Background: Photothermal therapy (PTT) has become an attractive approach for cancer treatment due to its merits of minimal invasiveness, location selectivity, and suitability for various cancer types. In PTT, photosensitizers are usually adopted to convert light to heat at tumor site, thereby generating heat-induced necroptosis or apoptosis. Therefore, the performance of photosensitizer (e.g., photothermal conversion efficiency (PCE), surface property, tumor accumulation and retention, etc.) determines the clinical manifestation of PTT. Currently, the poor tumor retention and potential long-term toxicity are two main obstacles for developing efficient photosensitizers. To address these issues, we have developed an in vivo tumor microenvironment stimuli-responsive self-assembled photosensitizer, which consists of a biomolecule, adenosine monophosphate (AMP) modified gold nanoparticles (AAu NPs), to enhance the accumulation and retention within tumor tissue for efficient PTT.

Results: The obtained AAu NPs with a hydrodynamic diameter of 9.12 ± 0.82 nm have excellent colloidal stability in aqueous solution. No sediments can be observed in the AAu NPs aqueous phase even after several months. The temperature of AAu aqueous suspension is elevated to 53.0 ℃ within 8 min at a low particle concentration of 80 μg/mL. A high PCE of 62.8% is obtained for AAu NPs based on the temperature change curves. The near-infrared (NIR) absorption and PCE of AAu NPs are enhanced compared to the surfactant-free Au NPs, enabling excellent photothermal cell-killing in vitro. When the AAu NPs arrive at the tumor tissue, they quickly form large aggregates via a collagen-induced assembly, leading to enhanced NIR absorption and improved tumor accumulation and retention, which enables a high PTT efficacy in vivo at a low photosensitizer dose of 40 μg and a low laser power density of 1.91 W/cm^2.

Conclusions: A collagen-induced self-assembled gold photosensitizer for efficient PTT has been synthesized based on a biomolecule, AMP modification method. The synthesized AAu NPs with high PTT efficacy, superior biosafety and fast excretion from the body is an effective therapeutic agent in photothermal cancer therapy.

Keywords: Adenosine monophosphate, Gold nanoparticles, Photothermal therapy, Melanoma, Collagen

Introduction

Photothermal therapy (PTT) that destroys cancer cells by heat-induced necroptosis or apoptosis has become an attractive cancer treatment modality due to its merits of minimal invasiveness, location selectivity, and suitability for various tumor types (Liu et al. 2019). In contrast to traditional tumor resection and chemotherapy, PTT precludes postoperative infections and anticancer drug-induced systematic side effects (Torpy et al. 2010). In PTT, the near-infrared (NIR) light that is poorly absorbed by biological tissues is converted efficiently to heat by photosensitizers whose characteristics such as NIR absorption, photothermal conversion efficiency (PCE) and surface property determine the clinical manifestation of PTT (Ali et al. 2019). To date, various organic/inorganic nanomaterials capable to convert light to heat can be used as PTT photosensitizers, such as polydopamine (PDA) (Lu et al. 2021), iron oxide (Li et al. 2017), carbon materials (Han et al. 2018; Lee and Gaharwar, 2020), black phosphor (Luo et al. 2019). Among them, plasmonic gold nanomaterials have received extensive attention due to its high stability, biocompatibility and absorption tenability (Goncalves et al. 2020; Guan et al. 2021). Specially, a variety of gold nanostructures including nanoshells, nanorods, nanocage and nanoassembly have shown enhanced NIR absorption by adjusting structure parameters such as shell thickness or aspect ratio (length/width) (Huang et al. 2013; Hu et al. 2006; Alkilany et al. 2012; Lal et al. 2008). Although tunable NIR absorption and encouraging PTT effectiveness have been demonstrated, these gold nanostructures still face challenges such as toxicity, pharmacokinetics, long-term biological behaviors in clinic applications (Ali et al. 2019). For example, robust particle structure and large particle size makes gold nanoshells and gold nanorods not likely to be fast excreted from the body, therefore causing long-term toxicity concerns (Gad et al. 2012). In addition, some toxic components adopted in syntheses of gold nanostructures (e.g., the cetyltrimethylammonium bromide (CTAB) surfactant in gold nanorod synthesis and the Ag self-sacrifice template in gold nanocage synthesis) may not be completely removed, which could bring toxicity in vivo and limit their clinical applications(Au et al. 2010; Huang et al. 2011). Therefore, ideal PTT photosensitizers for clinical uses should not only have effective PTT performance, but also have fast excretion from the body and superior biocompatibility to avoid short-term and long-term toxicity.

Biomolecule-stabilized gold nanoparticles are promising candidate in in vivo therapeutic applications due to their advantages such as excellent biocompatibility, high colloidal stability and ease in synthesis. However, their intrinsic absorption in NIR region is relatively weak, making it not ideal for PTT application where an 808 nm laser is commonly used for excitation. To enhance the NIR absorption, the self-assembly of gold nanoparticles into aggregates has been proposed as an effective strategy to red-shift the absorption peak. For example, gold aggregates have been prepared through incorporating gold nanoparticles into a series of biocompatible molecules including block copolymer (He et al. 2013), protein (Wang et al. 2019), and liposome (Rengan et al. 2015), which show successful red-shift in absorption and enhanced PTT efficacy. In spite of some advantages such as tunable absorption peak location by adjusting the gold nanoparticle distance in the aggregates, the pre-assembled aggregates with large size likely suffer from rapid clearance by the reticuloendothelial system, leading to poor tumor penetration and accumulation (Choi et al. 2007; Anselmo and Mitragotri, 2015). Besides,

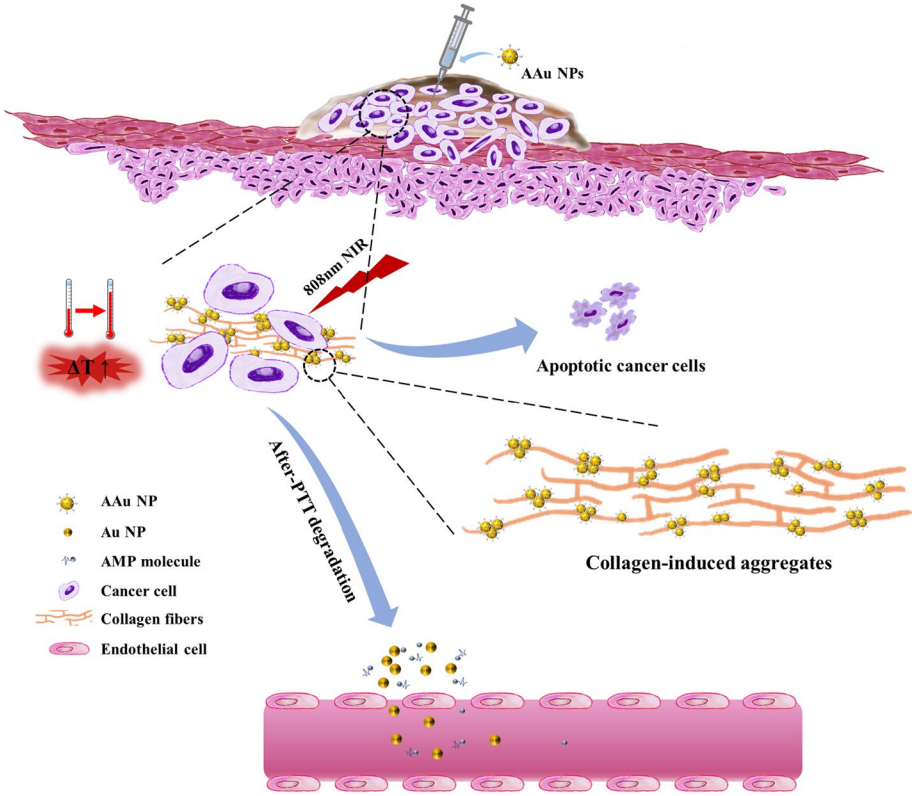

Scheme 1. Schematic illustration of collagen-induced aggregation of AAu NPs within tumor extracellular matrix for enhanced PTT

these pre-assembled aggregates may undergo a fast collapse due to degradation in tumor environment, leading to the rapid decrease in the efficacy of PTT. To circumvent these drawbacks of ex situ pre-assembled strategy, an in situ stimuli-responsive strategy has recently been developed to trigger self-assembly of gold nanoparticles within tumor tissues or tumor cells using various endogenous stimuli such as acidic pH (Yu et al. 2017; Liu et al. 2013a; Zhang et al. 2020), upregulated protein (Chen et al. 2020), and overexpressed enzyme (Yang et al. 2019, 2018). The gold nanoparticles keep well-isolated before entering tumor tissue while they will quickly self-assemble to aggregates upon being exposed to endogenous stimuli in tumor environment, endowing enhanced tumor accumulation and retention as well as fast systematical clearance. However, the current stimuli-responsive photothermal agents suffer from complex synthesis procedures, slow assembly process and low efficiency in stimuli-responsive aggregation due to insufficient expose of gold nanoparticles to the endogenous stimuli (e.g., insufficient gold nanoparticle amount taken up by tumor cells for intracellular assembly). Therefore, developing gold photosensitizers with fast and efficient stimuli-responsive aggregation within tumor is highly desirable for enhanced PTT, yet quite challenging.

In this article, we report on the design and synthesis of an in vivo tumor stimuli-responsive self-assembled gold nanoparticles (AAu NPs, Scheme 1) modified with a biomolecule, adenosine monophosphate (AMP) as effective photosensitizer for PTT. Collagen, as the main component of extracellular matrix in tumor tissues, is adopted as

the stimulus to trigger the self-assembly of AMP-modified Au nanoparticles (AAu NPs) within tumor tissue to enhance its accumulation and retention within tumor tissue for efficient PTT. The abundant collagen in the extracellular matrix allows sufficient interaction with the AAu agent, thereby resulting in high-efficiency and rapid stimuli-responsive aggregation under low agent dose. The AAu NPs have excellent colloidal stability in aqueous solution (e.g., phosphate buffered saline, PBS), but quickly self-assemble to aggregates once reaching tumor tissue due to the interaction between AAu NPs and collagen molecules. The in situ aggregated AAu NPs within tumor show higher absorption in NIR region due to enhanced localized surface plasmon resonance (LSPR) among adjacent Au atoms, which enhances its photothermal killing effect. Benefitting from the strong coordination between AMP active sites (e.g., NH_2 group) and Au atoms on the interface, the colloidal stability of AAu NPs is enhanced. Furthermore, the PTT performance of synthesized AAu photosensitizer for treating melanoma has been evaluated. The excellent effectiveness of tumor ablation demonstrates the advantages of collagen-induced in vivo self-assembly of Au NPs in the application of PTT.

Experimental section

Materials

$HAuCl_4$ and $NaBH_4$ were purchased from Aladdin (Shanghai, China). Adenosine 5′-monophosphate monohydrate (5′-AMP) was purchased from Sigma-Aldrich (USA). Phosphate buffered saline was purchased from Sangon Biotech (Shanghai, China). Dialysis bags were purchased from Shyuanye (Shanghai, China). High glucose medium was purchased from Hyclone (USA). Fetal bovine serum (FBS) was purchased from Epizyme (Shanghai, China). 3-(4,5-Dimethylthiazol-2-yl)-2,5-diphenyltetrazolium bromide (MTT) was purchased from Beyotime (Shanghai, China). The living and dead cell dyes were purchased from Solarbio (Beijing, China). The double antibody solution, collagen and trypsin were purchased from Gibco (USA). Paraformaldehyde was purchased from Biosharp (Hefei, China). BALB/Ca nude mice were purchased from Jihui Experimental Animal Breeding Co., Ltd. (Shanghai, China). All chemicals were used as received without any further purification.

Synthesis of AAu NPs

In a typical experiment, 1 mL $HAuCl_4$ (40 mmol/L) and 1 mL 5′-AMP (0.08 mmol/mL) were added into 8 mL distilled water at room temperature. After stirring for 30 min, 0.5 mL $NaBH_4$ (0.1 mmol/mL) was slowly added into the solution. The solution turned dark purple quickly and the product was obtained after continuous stirring for 30 min. The obtained solution was placed in a dialysis bag and dialyzed with distilled water or PBS for 3 days to obtain the AAu NPs suspension, which was stored at 4 ℃ for further characterization. The Au NPs were prepared as a control using the same procedure in the absence of AMP. Collagen-induced AAu NPs aggregates (CAAu) were obtained by adding 5 vol% 3 mg/mL collagen I colloid fluid to the obtained AAu NPs suspension.

Photothermal properties of AAu NPs

The AAu NPs suspensions with different concentrations (i.e., 8, 20, 40, 80 μg/mL) in the 96-well cell culture plate were irradiated by an 808 nm laser with a collimator (spot

size 0.785 cm^2) under different powers (0.5, 1, 1.5, 2, 2.5 W) for 10 min. The change of temperature was constantly recorded by an infrared camera. The temperature change of PBS was recorded as a control. Four laser on/off cycles were conducted to evaluate the photothermal stability of the AAu NPs (80 μg/mL, laser power 1.5 W). The photothermal curves of Au, AAu and CAAu samples at the same concentration of 80 μg/mL were measured upon irradiation by an 808 nm NIR laser (1.5 W) for 10 min.

In vitro photothermal cytotoxicity test

In vitro photothermal cytotoxicity tests were conducted using the MTT assay on mouse cutaneous melanoma (B16-F10) cell-line. Exponentially growing cells were seeded into 96-well plate (10^4 cells per well) and cultured overnight in 5% CO_2 humidified incubator at 37 °C for cell attachment. After being rinsed with PBS buffer (pH 7.4), the cells were treated with 100 μL of medium containing different concentrations of AAu NPs (0, 5, 10, 20, 40 μg/mL) for 24 or 48 h at 37 °C for evaluation of the materials cytotoxicity. For in vitro photothermal effect evaluation, the cells treated with different concentrations of AAu NPs (i.e., 0, 5, 10, 20, 40 μg/mL) for 2 h were irradiated with an 808 nm laser (laser power: 1.5 W; spot size: 0.785 cm^2) for 5 min. Different power densities (i.e., 0, 0.5, 1.5, 2.5 W) or irradiation time (i.e., 0, 0.5, 1, 2, 5, 10 min) were applied to the cells treated with 100 μL culture medium containing 20 μg/mL AAu NPs for dose-dependent photothermal effect evaluation. After laser irradiation, the cells were rinsed twice with PBS (pH 7.4) then the cell viability was measured using MTT assay by normalizing to control group without any treatment. To further evaluate the cell viability, the cells were stained with Calcein-AM/propidium iodide (PI) staining reagents immediately after laser irradiation and PBS cleaning. The stained cells were observed with fluorescence microscope at 494 nm (green, Calcein-AM) and 545 nm (red, PI). The results were all obtained from a representative experiment out of several biological replicates. Three parallel samples were conducted in each group.

In vivo antitumor experiment of Au–AMP

Female BALB/Ca mice, 5 weeks old, were used in the in vivo experiment. The animal experiments were approved by the Experimental Animal Ethics Committee of Shanghai Tenth People's hospital and all animal operations were in accord with institutional animal use and care regulations. The primary tumor model was established by subcutaneous injection of B16-F10 melanoma cells (2×10^6) into the right axillary of nude mice. Once the tumor volume reached about 60 mm^3, the tumor-bearing mice were randomly divided into 3 groups ($n = 4$), including (1) PBS; (2) AAu; and (3) AAu + Laser. Then, the three groups of mice were intratumorally injected with 500 μL of PBS or AAu NPs (80 μg/mL). After 10 min of intratumoral injection, the third group of mice were irradiated with an 808 nm laser (laser power: 1.5 W; spot size: 0.785 cm^2) for 10 min every 3 days (the nanoparticles were injected every 3 days before laser irradiation). Tumor volume and body weight were measured every 2 days. Tumor volume was calculated by the following equation: tumor volume = (length * $width^2$)/2. Ten days later, the mice were euthanized, and the tumors and the organs were collected for weighing, H&E staining, Ki67 staining and inductively coupled plasma-optical emission spectrometry (ICP) analysis.

Calculation of photothermal conversion efficiency

The photothermal conversion efficiency (η) of AAu NPs is calculated using the following formula:

$$\eta = \frac{hA\Delta T_{max} - Q_s}{I(1 - 10^{-A_\lambda})}, \tag{1}$$

where h is the heat transfer coefficient, A is the surface area of the container, $\Delta T_{\max}$ is the temperature change at the maximum steady-state temperature, I is the laser power, A_λ is the absorbance of AAu NPs at 808 nm, Q_S is the heat related to the light absorption of the solvent, which is independently measured as 25.2 mW by Yanlan Liu et al. (2013b).

In order to get hA in the formula (1), a dimensionless parameter θ is introduced as follows:

$$\theta = \frac{\Delta T}{\Delta T_{max}}. \tag{2}$$

Therefore, hA can be determined by applying the linear time data of cooling cycle versus $-\ln\theta$, as shown in the following:

$$t = \frac{\sum_i m_i c_{p,i}}{hA} \ln\theta \tag{3}$$

The photothermal conversion efficiency (η) of AAu can be calculated by substituting hA value into the formula (1).

Material characterization

The morphology of the AAu was observed using a transmission electron microscope (TEM, Hitachi H-800, Japan). Confocal laser scanning microscopy (CLSM, FV1000, Olympus Corporation, Japan) was used to observe the self-assembly of AAu NPs within extracellular matrix of tumor cells. The dynamic light scattering (DLS) of AAu in ultrapure water was measured using a Particle Size Analyzer (Zetasizernano, Malvern, UK). UV–Vis–NIR absorption spectra were recorded on a UV–Vis–NIR spectrometer (UV-3600, Shimadzu, Japan). X-ray powder diffraction (XRD) patterns were measured with an X'Pert PRO MPD powder diffractometer. Infrared absorption spectra are measured using an infrared spectrometer (FTIR-7600, Lambda Scientific, Australia). Thermal images were recorded by a near-infrared thermal imaging camera (FLIRTM A325SC camera) after irradiation using an 808 nm near-infrared laser equipment (Shanghai Connect Fiber Optics Company, China).

Statistical analysis

All data were expressed as mean ± standard deviation (SD). SPSS statistical software version 26 (IBM, Armonk, NY) was used for one-way ANOVA to determine the multiple comparisons between groups. $^{**}P < 0.01$ or $^{*}P < 0.05$ are significant differences.

Results and discussion

Structure of AAu NPs

AMP-modified gold nanoparticles (AAu NPs) were synthesized using sodium borohydride to reduce chloroauric acid in the AMP aqueous solution. The reduction reaction took place immediately upon mixing of two reactants, which was indicated by the color change of the solution. The XRD peaks that can be indexed to cubic Au phase (JCPDF 04-0784) show that the elemental gold nanoparticles are formed (Fig. 1A). Using the Scherrer's equation, the estimated grain size for AAu NPs is ~ 2.9 nm. TEM observations reveal that the particle size is 2.4 ± 0.6 nm (Fig. 1B). The particle size is comparable to the grain size, inferring that the AAu NPs are single crystals. The colloidal stability in aqueous media (i.e., distilled water) is preliminarily characterized by standing the suspension for months. The Au NPs without AMP modification quickly precipitate in the aqueous phase within half an hour. In contrast, no sediments can be observed in the AAu NPs aqueous phase even after several months, which indicates the AAu NPs have excellent colloidal stability (Fig. 1C). The hydrodynamic diameter of AAu NPs is measured by DLS to be 9.12 ± 0.82 nm (Fig. 1D). The colloidal stability of AAu NPs in different media for 7 days (i.e., distilled water, PBS, and PBS supplemented with FBS) is further characterized using DLS (Fig. 1D). The hydrodynamic diameters of AAu NPs in distilled water and PBS remain almost unchanged (i.e., ~ 9 nm) for 7 days, showing that the AAu NPs are stable in these media. In contrast, the hydrodynamic diameter increases from ~ 9 nm to ~ 55 nm for AAu NPs in the medium of PBS supplemented with FBS, indicating slight agglomeration occurs in the medium during 7 days. The agglomeration could be due to the binding effect between FBS molecules in the medium and AMP coating on the AAu NPs. The high colloidal stability is ascribed to the formation of a homogeneous

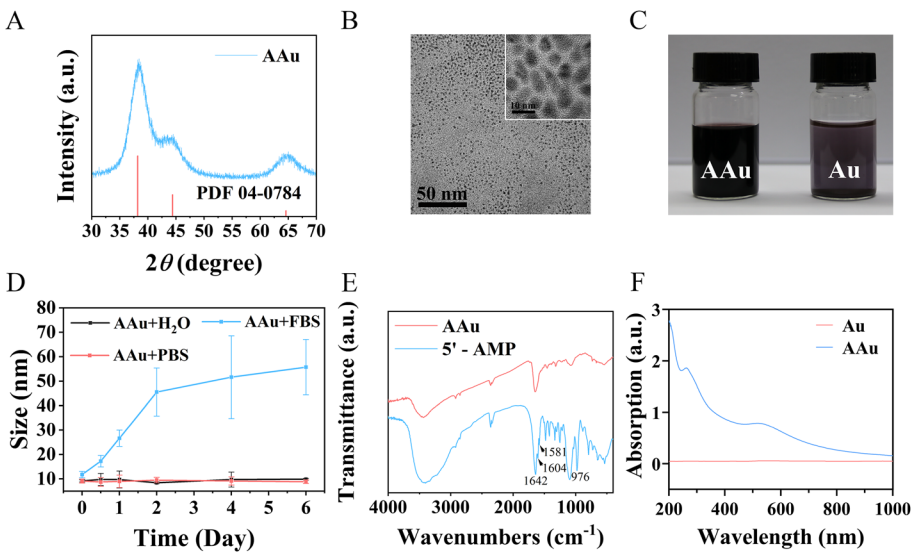

Fig. 1 Characterization of AMP-modified Au nanoparticles (AAu NPs). **A** XRD pattern. **B** TEM image. **C** Digital photos showing high colloidal stability of AAu NPs after standing for a month compared to surfactant-free Au NPs (the concentration of AAu and Au NPs are ~ 80 μg/mL). **D** Hydrodynamic diameters of AAu NPs in different media including distilled water, PBS, and PBS supplemented with FBS for 6 days. **E** FTIR curves of AAu NPs and AMP. **F** UV–Vis absorption curves of AAu and Au NPs at the diluted concentration (i.e., ~ 8 μg/mL)

AMP layer on the surface of Au NPs. During the reduction reaction, AMP molecules are coordinated to the surface Au atoms through N3 atom and/or the external NH_2 group to form a modification layer (Kundu et al. 2009). This structure can be proved by the negative Zeta potential (i.e., −22.6 mV) of AAu NPs suspension (Additional file 1: Figure S1). To ascertain the binding between AMP and Au, the FTIR are measured (Fig. 1E). The bands at 1604 cm^{-1} and 1581 cm^{-1} are merged with 1642 cm^{-1} (i.e., in-plane NH_2 scissor mode) to form one broad peak for the AAu NPs, indicating the strong binding between NH_2 and Au atom. In addition, the peaks at 976 cm^{-1} for symmetric stretching of the deprotonated terminal phosphate (Angell 1961) in AMP molecule are absent for AAu NPs, indicating that there is also interaction between phosphate and Au atom. As shown in Fig. 1F, the absorption in both visible and NIR regions of AAu NPs is evidently enhanced compared to surfactant-free Au NPs due to the enhanced colloidal stability of AAu NPs. The low absorption of Au NPs is because most of the Au NPs have settled down in the dilute solution during the measurement due to poor colloidal stability.

In vitro photothermal effect of AAu NPs

The photothermal effect of AAu NPs in PBS is evaluated using an 808 nm laser. The temperature of the AAu NPs suspension increases very quickly within 2 min and reaches a plateau after 8 min (Fig. 2A), showing a fast photothermal response of AAu NPs. The liquid temperature is raised to an equilibrium value of 36.7, 42.8, 48.6, and 53.0 ℃ at different AAu particle concentrations of 8, 20, 40, 80 μg/mL within 8 min (Fig. 2A). When the laser power is increased, the photothermal equilibrium temperature of AAu NPs suspension is elevated (Fig. 2B). An effective cell-killing temperature (i.e., > 42 ℃) can be achieved at a relatively low laser power of 1 W. These results show that AAu NPs have excellent photothermal effect with a concentration and laser power-dependent behavior.

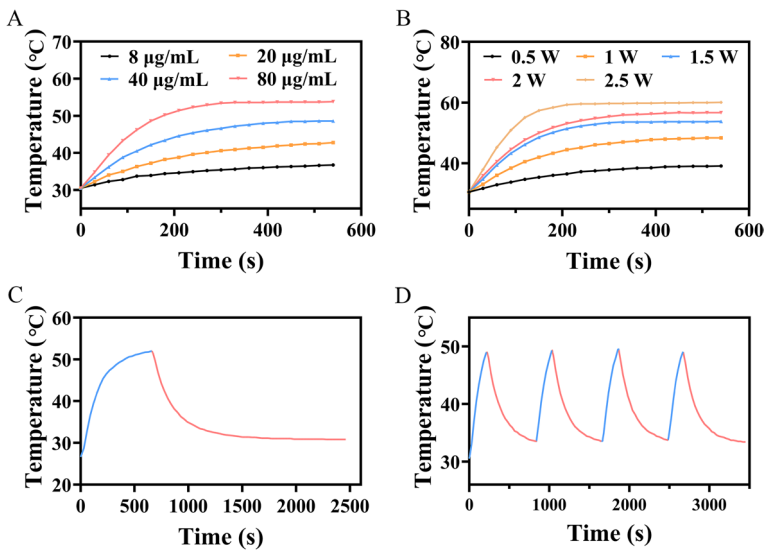

Fig. 2 Characterization of photothermal heating ability of AAu NPs. **A**, **B** Temperature elevation curves of AAu NPs suspensions upon laser irradiation as a function of irradiation time: **A** using different AAu NPs concentrations upon a laser irradiation power of 1.5 W; **B** using different laser power at a concentration of 80 μg/mL. **C** The photothermal response of AAu NPs suspensions tested by shutting off the laser after irradiation for 600 s. **D** Temperature changes of AAu NPs suspensions upon multiple laser on/off cycles

Based on the temperature change curves, the PCE of AAu NPs is calculated to be 62.8%. The PCEs of AAu NPs under different laser powers and different AAu concentrations are also investigated (Additional file 1: Figure S2). The PCE of AAu NPs maintains a high value of >50% at all these conditions. The high PCE is due to the reduced extinction of small size gold nanoparticles. The PCE is determined by the fraction of the absorption in the extinction (i.e., the sum of absorption and scattering), where the absorption is proportional to the nanoparticle volume while the scattering is proportional to the square of the nanoparticle volume. Thus, the smaller the nanoparticle, the higher the PCE becomes (Chen et al. 2010). Photothermal response curve shows that the elevated temperature of AAu NPs triggered by laser irradiation quickly decreases upon shutting off the laser, which can avoid undesired damage to normal tissue after PTT (Fig. 2C). Photothermal stability of photosensitizers is an important factor for PTT application. The photothermal stability of AAu NPs is evaluated by repeatedly turning on/off the laser (Fig. 2D). The temperature elevation remains the same for four cycles, indicating the high photostability of AAu NPs. The high photothermal effect of AAu NPs is likely due to (i) the high PCE due to the reduced extinction of the small size AAu NPs and (ii) the enhanced NIR absorption of our AAu NPs due to the high colloidal stability due to the strong coordination between AMP active sites (e.g., NH_2 group) and Au surface atoms. Combining these two aspects, our AAu NPs can absorb sufficient photon energy for light-to-heat conversion.

Collagen is the main component of extracellular matrix, which is also the component that AAu NPs will first come into contact with after entering tumor tissue. The collagen-induced self-assembly of AAu NPs is evaluated by co-incubation of AAu NPs with collagen for 120 min. After only 1 min incubation, AAu aggregates can be observed in the liquid phase (Fig. 3A). The self-assembly of AAu NPs in the presence of collagen is further confirmed by TEM images (Fig. 3B). The absorption spectrum of CAAu shows a red shift of the LSPR peak (from 510 to 515 nm) and an increase in intensity of the NIR region (Fig. 3C), which is ascribed to the strong plasmon coupling effect among AAu NPs induced by the reduced interparticle distance in the aggregates. The extinction coefficients of AAu and CAAu at both LSPR and 808 nm are calculated (Additional file 1: Table S1). The larger extinction coefficients of CAAu at 808 nm compared to that of AAu indicate that the CAAu has enhanced absorption ability in the NIR region. The small red shift (i.e., 5 nm) is probably because the surfaces of gold NPs could not fully interact in the CAAu sample due to the steric effects of collagen molecules. The improved NIR absorption of CAAu further enhances its photothermal effect in PBS, leading to a temperature rise of 3.8 ℃ compared to that of AAu (Fig. 3D). In contrast, a small increase in temperature of 19.9 ℃ is observed for surfactant-free Au NPs at the concentration of 80 μg/mL within the same time period, which is due to its poor absorption in the NIR region (Fig. 3D). No obvious temperature elevation is observed for the PBS solution (Fig. 3D). The significant increase in temperature upon laser irradiation at such a low concentration indicates that the AAu NPs have strong photothermal conversion ability. The photothermal effect stability of CAAu is further investigated by measuring temperature elevating curves in multiple NIR irradiation cycles (Additional file 1: Figure S3). The temperature reaches the same value after four laser on/off cycles as that under the first irradiation. After NIR irradiation, the AAu NPs in the CAAu sample remain aggregated

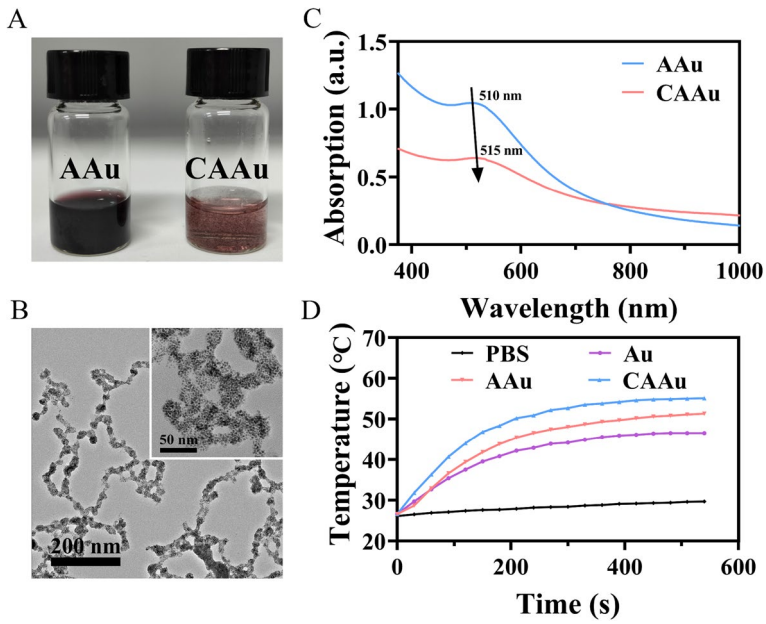

Fig. 3 Characterization of collagen-induced self-assembly of AAu NPs (CAAu). **A** Digital photos of AAu aqueous suspension and AAu aqueous suspension added with collagen (i.e., CAAu). **B** TEM images of CAAu. **C** The absorption spectra of AAu and CAAu. The LSPR peak shifts from 510 nm of AAu to 515 nm of CAAu. **D** Photothermal heating effects of Au, AAu and CAAu

in the collagen molecules which can absorb similar NIR photon energy to that before NIR irradiation (Additional file 1: Figure S4). These results show that the CAAu sample has stable PTT capacity.

We further investigate the in vitro photothermal effects of AAu NPs on B16-F10 cells. The cell viability is determined by normalizing to a control group. At all concentrations of co-incubating AAu NPs (i.e., from 5 to 40 μg/mL), the cell viability is > 90% and > 80% after 24 h and 48 h, showing excellent biosafety of our AAu photosensitizer (Fig. 4A). A series of snap photos at different time intervals show that the B16-F10 cells can actively grasp the AAu material, indicating the excellent biocompatibility of AAu NPs (Additional file 1: Figure S5). When laser irradiation is applied, the cell viability decreases with the increase of the AAu NPs concentration or the laser dose (i.e., laser power and irradiation time). Increasing laser dose (i.e., 1.5 W or 10 min) induces a dramatic drop in cell viability (Fig. 4B, C and Additional file 1: Figure S6). The cell viability decreases to ~ 40% and ~ 20% when the AAu NPs concentration reaches 20 μg/mL and 40 μg/mL upon laser irradiation of 1.5 W for 5 min. The cell-killing effect is due to the photothermal effect of our AAu NPs. The melanoma cells with melanin in the cells have negligible photothermal effect, which is proved by the literatures (Chen et al. 2018; Zhang et al. 2018; Wei et al. 2020). However, our laser power is higher than that used in the literatures. Under this condition, it may cause slight photothermal effects on melanoma. From the fluorescence images of dyed cells, homogeneous red fluorescence is observed upon applying relatively high particle concentration or laser dose, indicating that almost all cancer cells are killed (Fig. 4E and Additional file 1: Figure S6). From the Calcein-AM stained PBS group, one can see that the living cells have spherical shape with bright green color. In the

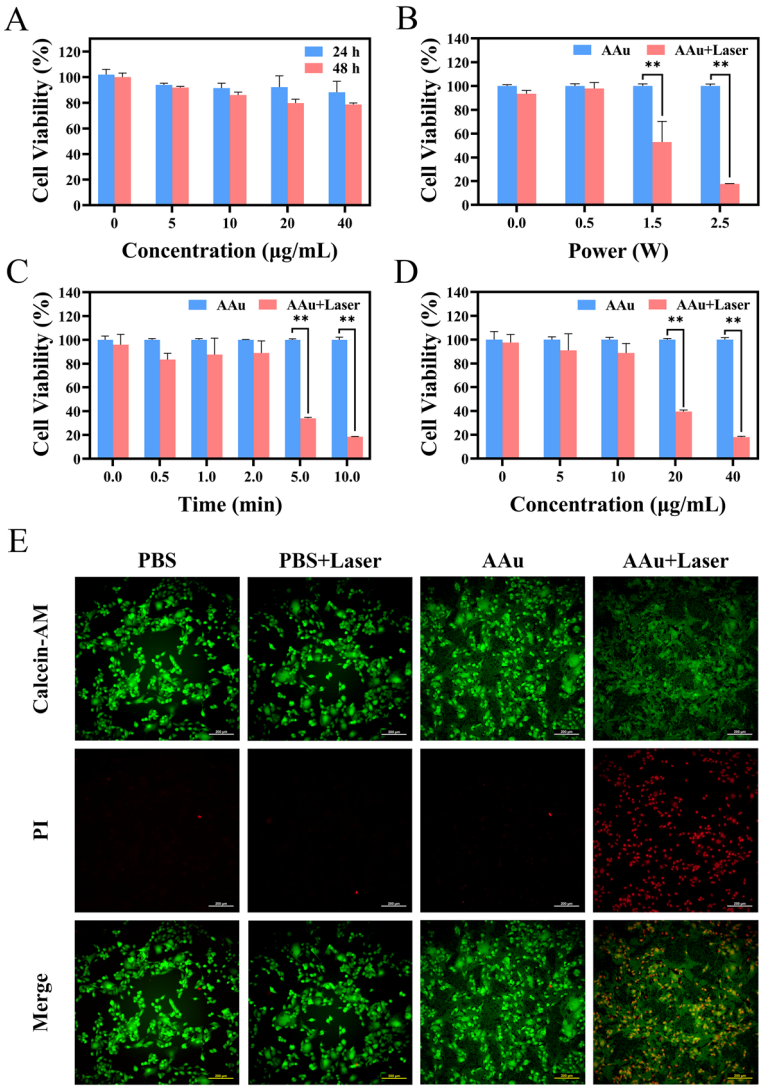

Fig. 4 In vitro photothermal effect of AAu NPs. **A** Cell viability of B16-F10 cells incubated with different concentrations of AAu NPs without laser irradiation. **B** and **C** Cell viability incubated with AAu NPs at a concentration of 20 μg/mL under laser irradiation with different power **B** or time **C**. **D** Cell viability incubated with AAu NPs at different concentrations after irradiation with an 808 nm laser (laser dose: 1.5 W, 5 min). **E** Fluorescent images of live (green) and dead cells (red) treated with PBS and AAu NPs. Scale bar: 200 μm. $^{**}P < 0.01$ or $^{*}P < 0.05$ are significant differences

Calcein-AM-stained AAu + Laser group, these spherical bright green areas are much decreased compared to the PBS, PBS + Laser and AAu groups. In the merged image, the red area and green area almost overlap. These results indicate that most cells are killed in the AAu + Laser group. (Fig. 4E). The results from both cell viability and fluorescence cell images show that AAu NPs have efficient and concentration/laser dose-dependent photothermal cytotoxicity to cancer cells. The extracellular aggregates of AAu NPs are also observed after co-incubation of AAu NPs with cell for 24 h (Additional file 1: Figure S5), which further confirms the collagen-induced assembly ability of the AAu NPs. The stimulus-responsive assembly of AAu NPs can promote the tumor accumulation and retention, which is beneficial for the in vivo PTT.

In vivo photothermal therapy evaluation of AAu NPs

The in vivo PTT performance of AAu photosensitizer is evaluated using a subcutaneous melanoma tumor-xenograft model. As the small nanometer-sized AAu photosensitizers would be easily excreted from the body or accumulated in the normal tissues, the preferred administration route for AAu NPs is intratumor injection. After grafting tumor for 2–3 days, once the tumor volume reaches about 60 mm^3, the treatment group of mice are intratumorally injected with 40 μg AAu NPs. Then an 808 nm laser irradiation of 1.5 W is applied on the tumor for 10 min (Additional file 1: Figure S8). The two control groups of mice are intratumorally injected with the same amount of PBS and AAu NPs without near-infrared illumination, respectively. An infrared camera is used to record the temperature change of the tumor site. Upon 808 nm laser irradiation, the temperature of the tumor administrated with AAu NPs increases up to 48.8 ℃ quickly within 2 min and further reaches 52.3 ℃ within 5 min (Fig. 5A), which is consistent with the temperature elevation curve in vitro. In contrast, the temperature remains almost unchanged in tumor injected with PBS. The tumor volume is monitored for 10 days

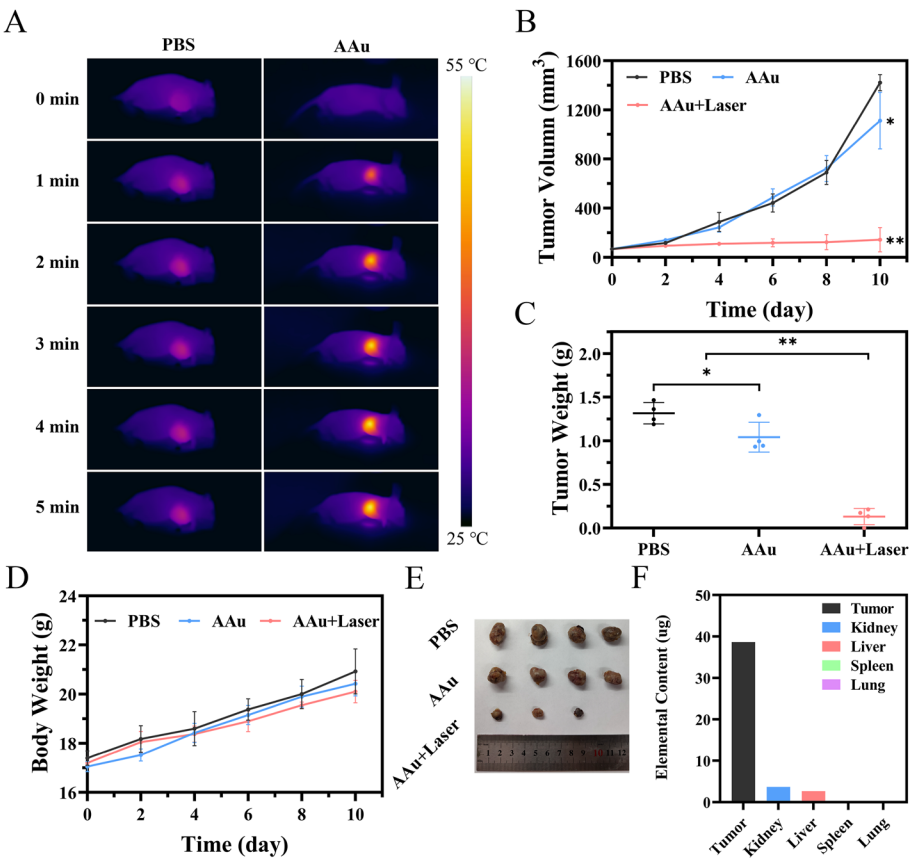

Fig. 5 Evaluation of collagen-induced assembled AAu NPs for in vivo photothermal therapy. **A** Temperature change in tumor under laser irradiation recorded by an infrared camera. **B** Tumor volume change in different groups for 10 days after treatment. *$P < 0.05$. **C** Tumor weight of different group after 10 days post-treatment. **D** Mouse weight change of different groups for 10 days after treatment. **E** Digital photograph of tumors taken out from mice in each group on day 10 after treatment. **F** Au elemental content of different organs taken from one mouse in the treatment group on the day 10 (i.e., 1 day after the last treatment). **$P < 0.01$ or *$P < 0.05$ are significant differences

after photosensitizer administration and laser irradiation. The unchanged tumor volume of the treatment group of mice for 10 days clearly shows that the AAu NPs-induced PTT effectively ablates the tumor (Fig. 5B). In contrast, the tumor of the control group administrated with AAu NPs starts to grow at a similar rate to that of the control group administrated with PBS after 2 days, indicating an insufficient tumor ablation (Fig. 5B and C). The stable weight of mice within 10 days indicates the excellent biosafety of AAu NPs (Fig. 5D). Clear cancer cell destruction is observed in the hematoxylin and eosin (H&E) staining and Ki-67 staining images of tumor slices after AAu NPs injection and laser irradiation, but is absent in the tumor tissues administrated with AAu NPs and PBS (Fig. 6A). The high PTT efficacy of AAu NPs could be due to three reasons including

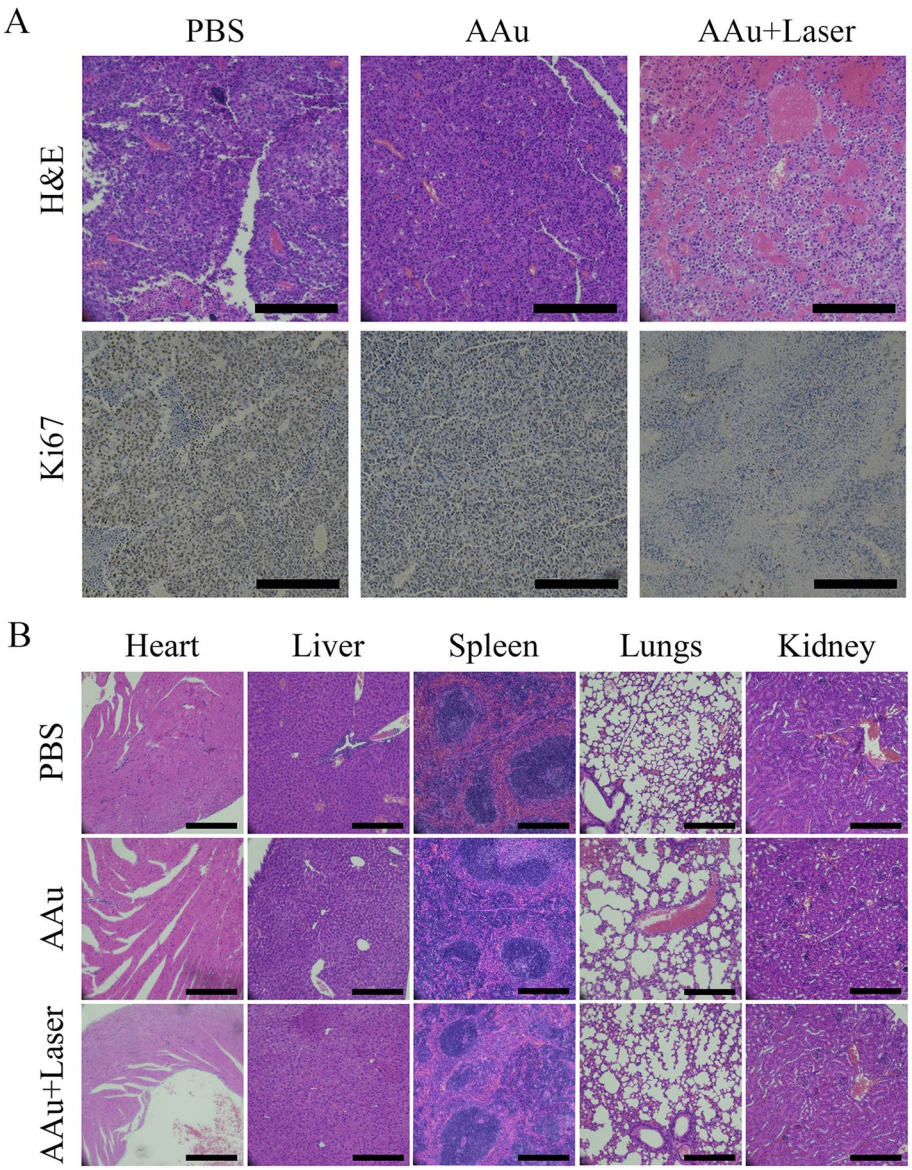

Fig. 6 **A** H&E stained and Ki-67 stained images of tumor slices in different groups. Scale bar: 400 μm. **B** H&E stained tissue images of different organs taken from mice in different groups on day 10 (i.e., 1 day after the last treatment). Scale bar: 400 μm

(i) promoted accumulation and prolonged retention in tumor of AAu NPs aggregates formed through collagen-induced self-assembly; (ii) enhanced NIR absorption of AAu NPs aggregates and (iii) high PCE of AAu NPs. The biodistribution of AAu NPs after injection for 10 days is evaluated. The histological analysis of different organs shows no significant damage of AAu NPs to these organs (Fig. 6B). One day after last treatment (i.e., day 10), a small portion of AAu NPs remains in tumor while most AAu NPs are excreted from the body since the negligible amount is observed in other organs (Fig. 5F and Additional file 1: Figure S9). These in vivo experiments further indicate that AAu NPs have remarkable PTT performance on tumors with excellent biosafety and fast clearance.

Summary

In summary, we have synthesized collagen-induced self-assembly gold photosensitizer for PTT based on a biomolecule, AMP modification method. The NIR absorption and PCE of AAu NPs after AMP modification are enhanced compared to the surfactant-free Au NPs, enabling excellent and durable in vitro photothermal cell-killing effect. The formation of AAu NPs aggregates through collagen-induced self-assembly promotes its accumulation and retention within tumor and further enhances the NIR absorption, which is beneficial for PTT application. Benefitting from the abundance of collagen in the extracellular matrix and its strong interaction with our AAu NPs, our strategy manifests high-efficiency stimuli-responsive aggregation with rapid aggregation time (i.e., within 1 min) and low agent dose (i.e., 80 μg/mL). The in vivo experiments show that AAu NPs have high PTT efficacy, superior biosafety and fast excretion from the body. This work may open a new avenue for the design and synthesis of effective therapeutic agents with high biosafety in photothermal cancer therapy.

Abbreviations

PTT	Photothermal therapy
AMP	Adenosine monophosphate
FBS	Fetal bovine serum
AAu NPs	AMP-modified gold nanoparticles
CAAu	Collagen-induced AAu NPs aggregates
CTAB	Cetyltrimethylammonium bromide
NIR	The near-infrared
PCE	Photothermal conversion efficiency
LSPR	Localized surface plasmon resonance
CLSM	Confocal laser scanning microscopy
TEM	Transmission electron microscopy
XRD	X-ray diffraction spectrum
FTIR	Fourier transform infrared spectrum
DLS	Dynamic light scattering
ICP	Inductively coupled plasma-optical emission spectrometry
MTT	3-(4,5-Dimethylthiazol-2-yl)-2,5-diphenyltetrazolium bromide
PI	Propidium iodide
SD	Standard deviation
PBS	Phosphate buffered saline

Supplementary Information

The online version contains supplementary material available at https://doi.org/10.1186/s12645-022-00130-1.

Additional file 1: Figure S1. Zeta potential of AAu sample. **Figure S2.** Photothermal conversion efficiency of the AAu sample at different laser powers and different AAu concentrations. **Figure S3.** Temperature changes of CAAu NPs suspensions upon multiple laser on/off cycles (808 nm, 1.5 W). **Figure S4.** (A) The TEM image and (B) absorption spectrum of the CAAu after irradiation with 808 laser for 10 min. **Figure S5.** Snap photos of B16-F10 cells after

co-incubation with AAu NPs for 24 h at different time intervals: (A) 0 s; (B) 1 s; (C) 2 s; and (D) 3 s, showing that the cell can actively grasp the AAu material, which indicates that the AAu NPs has good biocompatibility. **Figure S6.** The cytotoxicity of AAu to B16-F10 cells under near-infrared radiation was evaluated. (A) Fluorescent images of B16-F10 cells co-incubated with AAu NPs at the concentration of 20 μg/mL for 2 h with or without irradiation of an 808 nm NIR laser at various power densities (power: 0, 0.5, 1.5 and 2.5 W; spot size: 0.785 cm^2). (B) Fluorescent images of B16-F10 cells co-incubated with AAu NPs at various concentrations (i.e., 0, 5, 10, 20 and 40 μg/mL) for 2 h with or without laser irradiation (power: 1.5 W; spot size: 0.785 cm^2). (C) Fluorescent images of B16-F10 cells co-incubated with AAu NPs at the concentration of 20 μg/mL for 2 h with or without laser irradiation (power: 1.5 W; spot size: 0.785 cm^2) for various time (i.e., 0, 0.5, 1, 2, 5, 10 min). The cells were stained to show living (green) and dead cells (red) under fluorescence microscope. **Figure S7.** Fluorescent images of live (green) and dead cells (red) after co-incubation with AAu nanoparticles with various concentrations (i.e., 0, 5, 10, 20 and 40 μg/mL) for different time: (A) 24 h or (B) 48 h. Scale bar: 200 μm. **Figure S8.** Schematic illustration of the animal experimental design of the photothermal therapy for melanoma. **Figure S9.** The Au elemental concentration normalized to mass of different organs taken from one mouse on the day 10 (i.e., one day after the last treatment). The relatively high Au amount in kidney indicates that the AAu NPs can be excreted from the body through kidney due to its small size. **Table S1.** The calculated extinction coefficients (L·mmol−1·cm−1) of AAu and CAAu [1].

Acknowledgements
Not applicable.

Author contributions
XQ: conceptualization, methodology, investigation, data curation, writing—original draft. YC: data curation, formal analysis, methodology, investigation. ZC: methodology, validation, investigation. ZH: methodology, validation. XL: methodology, validation. ST: methodology, validation. BL: methodology, resources, project administration. RG: supervision, funding acquisition. XZ: methodology, validation, investigation, resources, project administration, funding acquisition and writing—original draft. FC: investigation, resources, project administration, funding acquisition. All authors read and approved the final manuscript.

Funding
This work was supported by the National Natural Science Foundation of China (31771081), the Science and Technology Commission of Shanghai Municipality (22S31903300, 21ZR1449700), Chenguang Program of Shanghai Municipal Education Commission (14CG37); Military Medical Science and Technology Youth Training Program (18QNP015) and the Foundation of Shanghai Talent Development Program (2021079).

Availability of data and materials
All data generated or analyzed during this study are included in this published article.

Declarations

Ethics approval and consent to participate
All animal experiments were approved by the Animal Ethics Committee of Shanghai Tenth People's Hospital Affiliated to TongJi University School of Medicine.

Consent for publication
All authors consent for publication.

Competing interests
All authors declared no competing interests.

Received: 1 February 2022 Accepted: 21 July 2022
Published online: 06 August 2022

References

Ali MRK, Wu Y, El-Sayed MA (2019) Gold-nanoparticle-assisted plasmonic photothermal therapy advances toward clinical application. J Phys Chem C 123:15375–15393
Alkilany AM, Thompson LB, Boulos SP, Sisco PN, Murphy CJ (2012) Gold nanorods: their potential for photothermal therapeutics and drug delivery, tempered by the complexity of their biological interactions. Adv Drug Deliv Rev 64:190–199
Angell CL (1961) 100. An infrared spectroscopic investigation of nucleic acid constituents. J Chem Soc. https://doi.org/10.1039/JR9610000504
Anselmo AC, Mitragotri S (2015) A review of clinical translation of inorganic nanoparticles. AAPS J 17:1041–1054
Au L, Chen J, Wang LV, Xia Y (2010) Gold nanocages for cancer imaging and therapy. In: Grobmyer SR, Moudgil BM (eds) Cancer nanotechnology methods and protocols. Humana Press, Totowa
Chen J, Ma Y, Du W, Dai T, Wang Y, Jiang W, Wan Y, Wang Y, Liang G, Wang G (2020) Furin-instructed intracellular gold nanoparticle aggregation for tumor photothermal therapy. Adv Funct Mater 30:2001566
Chen W, Qin M, Chen X, Wang Q, Zhang Z, Sun X (2018) Combining photothermal therapy and immunotherapy against melanoma by polydopamine-coated Al_2O_3 nanoparticles. Theranostics 8:2229–2241

Chen H, Shao L, Ming T, Sun Z, Zhao C, Yang B, Wang J (2010) Understanding the photothermal conversion efficiency of gold nanocrystals. Small 6:2272–2280
Choi HS, Liu W, Misra P, Tanaka E, Zimmer JP, Ipe BI, Bawendi MG, Frangioni JV (2007) Renal clearance of quantum dots. Nat Biotechnol 25:1165–1170
Gad SC, Sharp KL, Montgomery C, Payne JD, Goodrich GP (2012) Evaluation of the toxicity of intravenous delivery of auroshell particles (gold-silica nanoshells). Int J Toxicol 31:584–594
Goncalves ASC, Rodrigues CF, Moreira AF, Correia IJ (2020) Strategies to improve the photothermal capacity of gold-based nanomedicines. Acta Biomater 116:105–137
Guan G, Win KY, Yao X, Yang W, Han M-Y (2021) Plasmonically modulated gold nanostructures for photothermal ablation of bacteria. Adv Healthc Mater 10:2001158
Han B, Zhang Y-L, Chen Q-D, Sun H-B (2018) Carbon-based photothermal actuators. Adv Funct Mater 28:1802235
He J, Huang X, Li Y-C, Liu Y, Babu T, Aronova MA, Wang S, Lu Z, Chen X, Nie Z (2013) Self-assembly of amphiphilic plasmonic micelle-like nanoparticles in selective solvents. J Am Chem Soc 135:7974–7984
Hu M, Chen J, Li Z-Y, Au L, Hartland GV, Li X, Marquez M, Xia Y (2006) Gold nanostructures: engineering their plasmonic properties for biomedical applications. Chem Soc Rev 35:1084–1094
Huang P, Bao L, Zhang C, Lin J, Luo T, Yang D, He M, Li Z, Gao G, Gao B et al (2011) Folic acid-conjugated Silica-modified gold nanorods for X-ray/CT imaging-guided dual-mode radiation and photo-thermal therapy. Biomaterials 32:9796–9809
Huang P, Lin J, Li W, Rong P, Wang Z, Wang S, Wang X, Sun X, Aronova M, Niu G et al (2013) Biodegradable gold nanovesicles with an ultrastrong plasmonic coupling effect for photoacoustic imaging and photothermal therapy. Angew Chem Int Ed 52:13958–13964
Kundu J, Neumann O, Janesko BG, Zhang D, Lal S, Barhoumi A, Scuseria GE, Halas NJ (2009) Adenine- and adenosine monophosphate (AMP)-gold binding interactions studied by surface-enhanced raman and infrared spectroscopies. J Phys Chem C 113:14390–14397
Lal S, Clare SE, Halas NJ (2008) Nanoshell-enabled photothermal cancer therapy: impending clinical impact. Acc Chem Res 41:1842–1851
Lee HP, Gaharwar AK (2020) Light-responsive inorganic biomaterials for biomedical applications. Adv Sci 7:2000863
Li J, Wang S, Shi X, Shen M (2017) Aqueous-phase synthesis of iron oxide nanoparticles and composites for cancer diagnosis and therapy. Adv Colloid Interface Sci 249:374–385
Liu X, Chen Y, Li H, Huang N, Jin Q, Ren K, Ji J (2013a) Enhanced retention and cellular uptake of nanoparticles in tumors by controlling their aggregation behavior. ACS Nano 7:6244–6257
Liu Y, Ai K, Liu J, Deng M, He Y (2013b) Lu LJAm: dopamine-melanin colloidal nanospheres: an efficient near-infrared photothermal therapeutic agent for in vivo cancer therapy. Adv Mater 25:1353–1359
Liu Y, Bhattarai P, Dai Z, Chen X (2019) Photothermal therapy and photoacoustic imaging via nanotheranostics in fighting cancer. Chem Soc Rev 48:2053–2108
Lu J, Cai L, Dai Y, Liu Y, Zuo F, Ni C, Shi M, Li J (2021) Polydopamine-based nanoparticles for photothermal therapy/chemotherapy and their synergistic therapy with autophagy inhibitor to promote antitumor treatment. Chem Rec 21:781–796
Luo M, Fan T, Zhou Y, Zhang H, Mei L (2019) 2D Black phosphorus-based biomedical applications. Adv Funct Mater 29:1808306
Rengan AK, Bukhari AB, Pradhan A, Malhotra R, Banerjee R, Srivastava R, De A (2015) In vivo analysis of biodegradable liposome gold nanoparticles as efficient agents for photothermal therapy of cancer. Nano Lett 15:842–848
Torpy JM, Burke AE, Glass RM (2010) JAMA patient page postoperative infections. Jama 303:2544–2544
Wang J, Zhang Y, Jin N, Mao C, Yang M (2019) Protein-induced gold nanoparticle assembly for improving the photothermal effect in cancer therapy. ACS Appl Mater Interfaces 11:11136–11143
Wei S, Quan G, Lu C, Pan X, Wu C (2020) Dissolving microneedles integrated with pH responsive micelles containing AIEgen with ultraphotostability for enhancing melanoma photothermal therapy. Biomater Sci 8:5739–5750
Yang K, Liu Y, Wang Y, Ren Q, Guo H, Matson JB, Chen X, Nie Z (2019) Enzyme-induced in vivo assembly of gold nanoparticles for imaging-guided synergistic chemo-photothermal therapy of tumor. Biomaterials 223:119460
Yang S, Yao D, Wang Y, Yang W, Zhang B, Wang D (2018) Enzyme-triggered self-assembly of gold nanoparticles for enhanced retention effects and photothermal therapy of prostate cancer. ChemComm 54:9841–9844
Yu Z, Wang M, Pan W, Wang H, Li N, Tang B (2017) Tumor microenvironment-triggered fabrication of gold nanomachines for tumor-specific photoacoustic imaging and photothermal therapy. Chem Sci 8:4896–4903
Zhang R, Wang L, Wang X, Jia Q, Chen Z, Yang Z, Ji R, Tian J, Wang Z (2020) Acid-induced in vivo assembly of gold nanoparticles for enhanced photoacoustic imaging-guided photothermal therapy of tumors. Adv Healthc Mater 9:2000394
Zhang Y, Zhan X, Xiong J, Peng S, Huang W, Joshi R, Cai Y, Liu Y, Li R, Yuan K, Zhou N, Min W (2018) Temperature-dependent cell death patterns induced by functionalized gold nanoparticle photothermal therapy in melanoma cells. Sci Rep 8:8720

Publisher's Note